AIAA JOURNAL
Vol. 48, No. 3, March 2010

Experimental Investigation of Flow Separation Control Using an Array of Synthetic Jets

Shanying Zhang* and Shan Zhong†
University of Manchester, Manchester, England M60 1QD, United Kingdom

DOI: 10.2514/1.43673

An experimental study of flow control using an array of three synthetic jets has been undertaken in a separated laminar flow over an inclined flat plate in a water channel. Particle image velocimetry was employed to obtain the information about the extent of flow separation delay at different synthetic jet operating conditions. A laser-induced florescence flow visualization technique was used to reveal the characteristics of the vortical structures produced by the synthetic jets, which result in a delay of separation. It was observed that the flow separation delay is typically associated with the presence of two or three streaks of high streamwise velocity in the separated flow. Based on the results from the present experiment, a parameter map indicating the flow patterns observed at different synthetic jet operating conditions is produced. In addition, a contour map showing the separation control effectiveness at the corresponding conditions is also obtained. It was found that the two-streak flow pattern is mostly produced at a jet-to-freestream velocity ratio between 0.3 and 0.5, whereas the three-streak pattern occurs at a velocity ratio between 0.5 and 1.5. The laser-induced florescence images confirm that the two-streak flow pattern is caused by the hairpin type vortical structures produced by synthetic jets, whereas the three-streak pattern is caused by the tilted vortex ring type structures. For the range of actuator operating conditions tested in this study, operating the synthetic jets at a dimensionless stroke length of around 2, a velocity ratio of around 0.5, and a Strouhal number of around 1.6 would deliver the best flow control effect with the least energy consumption. Under these conditions, hairpinlike vortical structures are observed with a streamwise spacing of 44% of the local boundary-layer thickness at the orifices of the synthetic jets. In this experiment, the spacing between the jets and the distance between the jet array and the baseline separation line are fixed. As the level of interaction between neighboring synthetic jets and their flow control effectiveness are expected to alter upon changes in these two parameters, the generality of this finding remains to be established in future work.

Nomenclature

C	=	length of the inclined plate, mm
D	=	diameter of cavity or orifice, mm
f	=	diaphragm oscillation frequency, Hz
L	=	dimensionless stroke length
Re_L	=	Reynolds number based on dimensionless stroke length
Str	=	Strouhal number
T	=	time period of diaphragm oscillation cycle, s
U	=	characteristic velocity, m/s
x	=	streamwise distance, mm
y	=	normal distance from wall, mm
z	=	spanwise distance from centerline, mm
Δ	=	peak-to-peak displacement at the diaphragm center, mm
δ	=	boundary-layer thickness, mm
ρ	=	fluid density, kg/m^3
ν	=	molecular kinematic viscosity, m^2/s

Subscripts

c	=	cavity value
o	=	orifice value
∞	=	freestream value

Superscripts

$\bar{}$	=	time average

Presented as Paper 4185 at the 39th AIAA Fluid Dynamics Conference, San Antonio, TX, 22–25 June 2009; received 9 February 2009; revision received 11 November 2009; accepted for publication 28 November 2009.

*Research Associate, School of Mechanical, Aerospace and Civil Engineering, Sackville Street.

†Senior Lecturer, School of Mechanical, Aerospace and Civil Engineering, Sackville Street. Senior Member AIAA.

I. Introduction

SYNTHETIC jet actuators have been regarded as a promising method of delivering flow control for aircraft applications due to their ability to inject momentum to an external flow without net mass flux [1–3] and their potential in being integrated in microfabricated electromechanical systems through microfabrication with relative ease [4–6]. It has been demonstrated in many laboratory experiments that synthetic jets are capable of delaying flow separation on aerodynamic bodies of various shapes [1,7–9]. To the knowledge of the authors, however, almost all flow control experiments reported so far have been undertaken by setting the operating conditions of the actuators by trial and error. As a result, the actuator operating conditions, such as the jet-to-freestream velocity ratio, that are reported as being effective vary greatly from one experiment to another [7,10,11] and the level of flow control effectiveness has been observed to vary in an unpredictable manner with different geometric and injection parameters. To design effective flow control devices that are capable of delivering a required flow control effect at minimum energy expenditure, a better understanding of the fluid mechanics of the interaction between synthetic jets and a boundary layer is required.

Existing experimental evidence shows that the interaction of the train of vortices produced by a circular synthetic jet with a boundary layer results in the formation of streamwise vortical structures, which are capable of delaying flow separation by entraining faster-moving fluid from the freestream to the near-wall region [7]. To obtain a better understanding of the nature of these vortical structures, both experimental and numerical simulations have been undertaken on a single circular synthetic jet issued into a zero-pressure-gradient boundary layer [12–14]. It is shown that, as the dimensionless jet stroke length and the jet-to-freestream velocity ratio increases, the primary vortical structures produced by the interaction between the

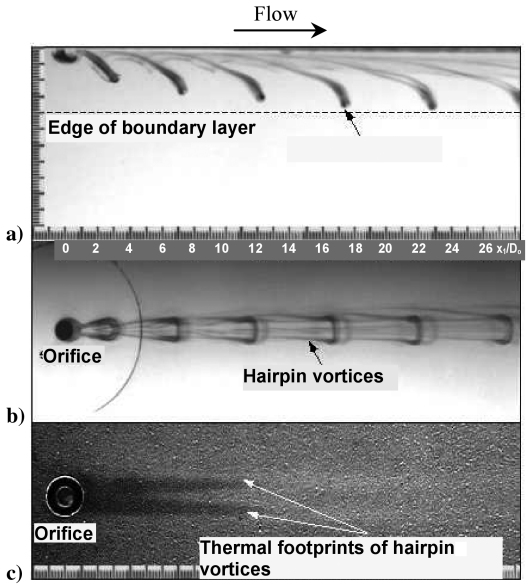

Fig. 1 Hairpin vortices: a) dye visualization images, side view; b) dye visualization images, top view; and c) thermal footprints.

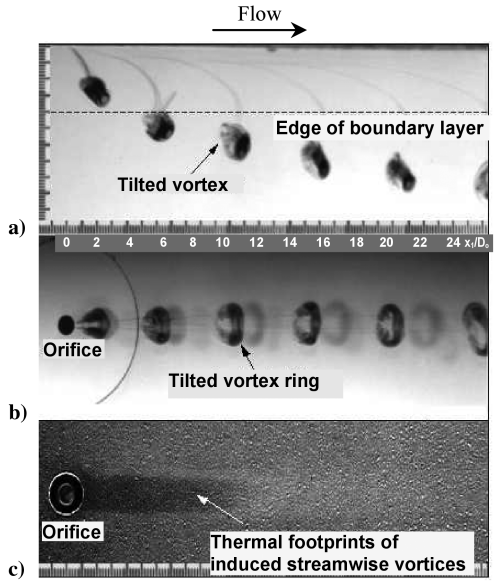

Fig. 2 Tilted vortex rings: a) dye visualization images, side view; b) dye visualization images, top view; and c) thermal footprints.

synthetic jet and the boundary layer first appear as hairpinlike vortices that are located close to the wall (Figs. 1a and 1b) and then as tilted vortex rings that penetrate the edge of the boundary layer shortly downstream (Fig. 2a and 2b). Using a temperature-sensitive liquid crystal surface coating, Jabbal and Zhong [12] found that the hairpin type structures produce a pair of streamwise streaks associated with a high heat transfer rate downstream of the orifice (Fig. 1c), whereas the tilted vortex ring type structures produce a single streamwise streak directly downstream of the orifice (Fig. 2c). By the Reynolds Analogy, an area of high heat transfer rate is associated with a local high wall shear stress or a local high flow velocity in the near-wall region.

According to Jabbal and Zhong [12], the hairpin vortex is formed as a result of the upstream branch of the vortex ring produced by the synthetic jet being first weakened by the suction cycle as it passes over the orifice and then subsequently being cancelled out by the resident vorticity of the opposite sign as it propagates downstream. Note that, if the initial strength of the vortex ring as it is formed at the orifice exit is relatively strong, the vortical structures may appear as a stretched vortex ring with a weak upstream branch in the near field before it turns into a hairpin structure further downstream. The presence of hairpin vortices is also confirmed in the computational fluid dynamics (CFD) simulations of Zhou and Zhong [13], who found that the legs of the hairpins trailing along the wall also induce a pair of streamwise vortices of the opposite sign outboard. The legs of hairpins and their induced streamwise vortices together create a downwash that brings high-speed fluid from the outer part of the boundary layer to the wall; see Fig. 3a. Consequently, each hairpin vortex produces a pair of high-speed streaks in the near-wall region, as shown in Fig. 3b.

At a higher velocity ratio and dimensionless stroke length, the vortex rings produced by the synthetic jets are able to escape from the impact of the suction cycle and the resident shear in the boundary layer and hence emerge as complete rings. The vortex rings appear to be tilted relative to the wall. They are located outside the boundary layer and connected to the wall via a pair of counter-rotating legs. According to Zhou and Zhong [13], the counter-rotating legs further induce a pair of tertiary streamwise vortices of an opposite sense directly underneath, as shown in Fig. 4a. This pair of tertiary streamwise vortices produces a downwash that brings high-speed fluids to the near-wall region on the central plane of the orifice. Consequently, each tilted vortex ring structure produces a single high-speed streak in the near-wall region; see Fig. 4b.

Jabbal and Zhong [12] also presented a map of parameter space where the different types of vortical structures were observed based on the Reynolds number and dimensionless stroke length of the synthetic jet. They hypothesized that the hairpin type structures would be favorable for flow separation control in view of their persistent wall shear stress signature in the boundary layer and the relatively lower level of power consumption required for producing them.

On the basis of understanding the interaction of a single synthetic jet with a zero-pressure-gradient boundary layer, the work reported in this paper goes one step further by applying an array of synthetic jets to a separated laminar boundary layer over an inclined flat plate in a water flow experiment. Particle image velocimetry (PIV) measurements made on a plane parallel to the inclined plate in the vicinity of its surface were carried out to provide quantitative information about the control effect of synthetic jets operating at different actuation conditions on the separated boundary layer. The laser-induced florescence (LIF) images taken on the streamwise central plane of the synthetic jet are used to assist the interpretation of the general characteristics of the vortical structures that are responsible for the delayed separation. The aim of this work is to identify the synthetic jet operating conditions and the type of vortical structures that could yield the best flow control effect.

To simplify the measurements, the present study was undertaken in a laminar boundary layer. However, the authors believe that the finding from this work would be still useful to the design of synthetic jet actuators for flow control at practical settings because some commonalities exist in the interaction mechanisms between synthetic jets and a boundary layer regardless of whether it is laminar or turbulent. First, the basic effect of shear in a boundary layer and the effect of suction cycle on the formation of coherent structures produced by synthetic jets in the boundary layer are similar regardless of whether the boundary layer is laminar or turbulent. Second, the entrainment brought about by the coherent vortices produced by the synthetic jets is an important flow separation mechanism in both flows. In the authors' opinion, understanding the behavior of synthetic jets in a laminar flow is the first logical step toward understanding the more complex behavior of synthetic jets in a turbulent flow.

II. Experimental Facilities and Methods

A. Water Flume and Test Plate

The experiments were conducted in a tilting flume located at the Goldstein Aeronautical Laboratory at Manchester University. The test section of the flume is about 4 m long with a cross section of 0.3×0.3 m^2. A uniform steady flow with a velocity up to 0.4 ms^{-1} can be achieved in the test section.

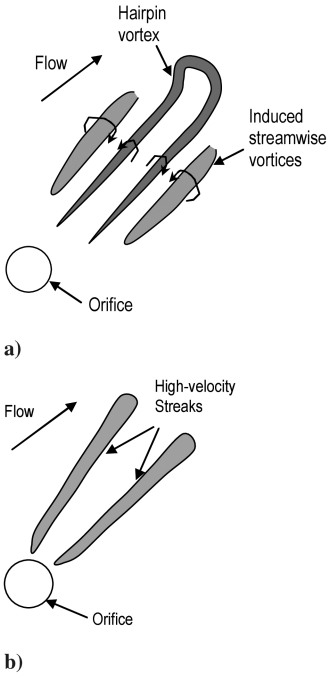

Fig. 3 Schematic drawings: a) hairpin vortex and its induced streamwise vortices produced by a single synthetic jet, and b) high-speed streaks produced by the single synthetic jet.

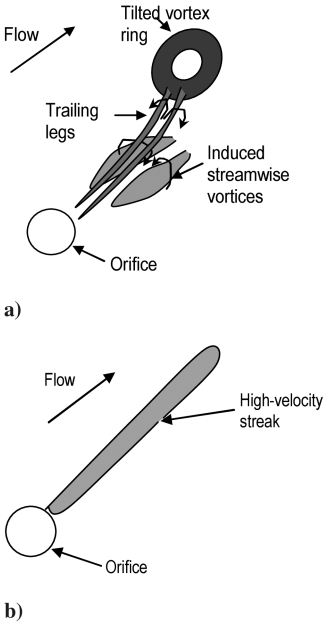

Fig. 4 Schematic drawings: a) tilted vortex ring and its secondary and tertiary structures produced by a single synthetic jet, and b) high-speed streaks produced by the single synthetic jet.

Figure 5a shows the sketch of the test plate and its coordinate systems. The test plate consists of three 11-mm-thick aluminum flat plates, each having the same width as the test section. They are connected to each other sequentially using hinges. The test surface faces downward to allow the synthetic jets actuator to be mounted above the free surface of water. The most upstream plate is 530 mm in length with an elliptical leading edge. It is mounted horizontally across the whole width of the test section. The spreading of the sidewall contamination is reduced by leaving a small gap between the side edges of the flat plate and the test section walls so as to maximize the portion of two-dimensional flow over the test surface. The evidence, that the separated flow in the baseline case is two dimensional across the interaction zone between the synthetic jets and the separated boundary layer, can be seen in the PIV results shown in Fig. 8b, which will be discussed later. The middle plate is 200 mm in length and it is inclined 5 deg upward relative to the horizontal plane. The boundary layer developing along the horizontal plate will separate at some point along the inclined plate, creating a separated boundary layer to which flow control with synthetic jets can be applied. Finally, a 150-mm-long plate is attached to the end of the inclined plate. The incidence angle of this plate can be altered to ensure that the flow is attached at the leading edge of the horizontal plate.

B. Synthetic Jet Array

The synthetic jet array consists of three jets that are issued through three circular orifices aligned normally to the flow direction on the test surface. The orifices have a diameter of $D_o = 2$ mm and a depth of 3 mm (see Fig. 5b). The three jets are produced by an oscillating diaphragm attached to a single cylindrical cavity with a diameter of 45 mm and a height of 12 mm. The diaphragm is made of a thin rubber sheet that is sandwiched between two thin metal disks. The rubber sheet is clamped circumferentially to the back of the cylindrical cavity. The center of the diaphragm is attached to a permanent magnetic shaker via a steel rod and it is made to oscillate in a sinusoidal manner at predetermined oscillation displacements and frequencies. With this arrangement, the diaphragm essentially mimics a pistonlike motion.

The intention of this work is to study the interaction of a synthetic jet array with a separated boundary layer. An array of three jets contains the minimum number of jets that allow such an interaction to be studied with the middle jet closely representing a typical jet in an array. In this experiment, to focus on the study of the flow control effect of changing actuator operating conditions, the jet spacing and the distance between the jet array and the baseline separation line are fixed. The array is located at 450 mm downstream of the leading edge of the horizontal plate, leaving a distance of 80 mm to the start of the inclined plate ($40D_o$) and a distance of about 120 mm to the baseline separation line ($60D_o$). The spacing between synthetic jets is fixed at 12 mm ($6D_o$).

In this experiment, the jet spacing of $6D_o$ is dictated by the actuator geometry as it is about the maximum spacing for a cavity diameter of 45 mm without making the two side orifices too close to the cavity wall. A comparison of the dye trajectories of the middle synthetic jet of the array and those of a single jet at the same dimensionless parameters revealed a very little difference, implying that the interaction between the adjacent synthetic jets at this spacing is negligible. As such, the finding obtained for single jets in previous works [12–14] can provide a basis for interpreting the results of the jet array.

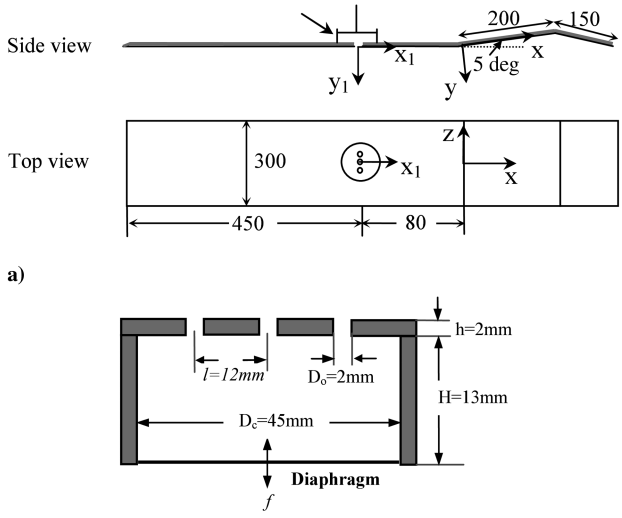

Fig. 5 Schematic drawings: a) test plate and coordinate system (units in millimeters), and b) synthetic jet actuator.

C. Laser-Induced Florescence

In the present study, the laser-induced florescence technique was employed to visualize the vortical structures produced by the interaction between the synthetic jets and the boundary layer. The florescent dye was injected into the cavity of the synthetic jet actuator by gravity. A laser sheet from a pulsed Nd:YAG laser was used to illuminate the streamwise plane that bisected the central orifice in the jet array. The LIF images were recorded using a TSI 4 megapixel PIV camera.

D. Particle Image Velocimetry

PIV measurement was undertaken to provide quantitative information about the control effect of synthetic jets on the separated boundary layer. To reveal the highly three-dimensional interaction between the synthetic jets and the separated flow over the inclined plate, the measurement was made on a spanwise plane parallel to the inclined plate. The 1-mm-thick laser light sheet, generated by a 5 W argon ion continuous laser, was located at a distance of about 1.5 mm below the plate so as to keep the surface reflection to a manageable level. In each test case, 100 successive images were taken at 30 Hz using a 1 megapixel Hitachi KP-F120 charge-coupled device camera. The images were postprocessed to obtain the time-averaged velocity field of the separated flow using the TSI Insight 3G PIV software. The choice of the number of images used in the averaging is a compromise between the computational time required and the desired smoothness of the time-averaged flowfield. Based on the published work from Jabbal and Zhong [12], an average of 100 images is sufficient for laminar flows such as those studied in this work.

The viewing area was chosen to be 160×160 mm^2 beginning from the start of the inclined plate. With a 16×16 pixel interrogation area, the spatial resolution is 2.5 mm in both the streamwise and spanwise directions. The uncertainty of the velocity measurement is about 5×10^{-4} m/s, which is equivalent to 2.5% of the local time-averaged velocity in the undisturbed boundary layer. In the present experiment, the spatial resolution has to be compromised due to the need for measuring a separated flow region that is as large as possible. However, as the measurement is taken in the separated flow region more than $40D_o$ downstream of the orifices, the vortical structures have already grown considerably in size in the spanwise direction. In addition, they also become more diffused as a result of the interaction with the separated flow. As such, even with a PIV interrogation area twice as large, the velocity contour and vector field still appear almost identical. Figure 6 shows the streamwise velocity fluctuations across the span at two streamwise locations on the inclined plate at $f = 12$ Hz and $L = 2$, where a typical two high-speed streak pattern to be explained in Sec. IV.C is observed. The fact that the strength of the high-speed streaks is substantially larger than the random uncertainty of the PIV measurements confirms that the setup used in this PIV experiment produces credible velocity data.

III. Test Conditions

A. Flow Conditions

All the tests in this study were performed at a freestream velocity of 0.1 m/s. The freestream turbulent intensity was about 0.3%. The velocity profiles of the boundary layer were extracted from the

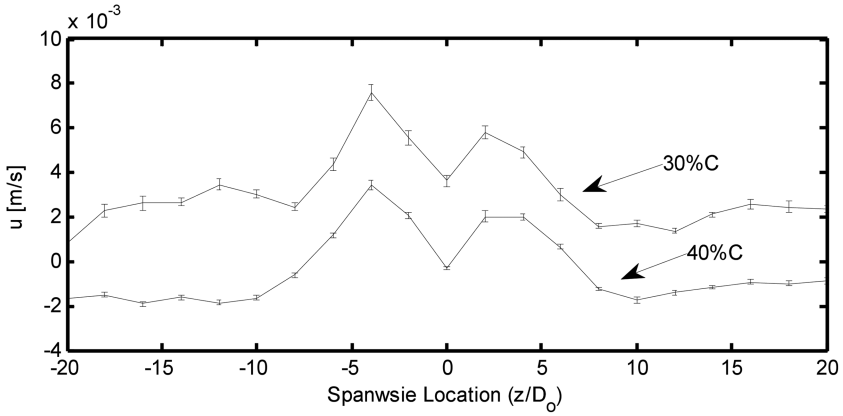

Fig. 6 Time-averaged streamwise velocity fluctuations across the span at two streamwise locations on the inclined plate at $f = 12$ Hz and $L = 2$ showing the high-speed streaks caused by the synthetic jets and the error bars of PIV measurements.

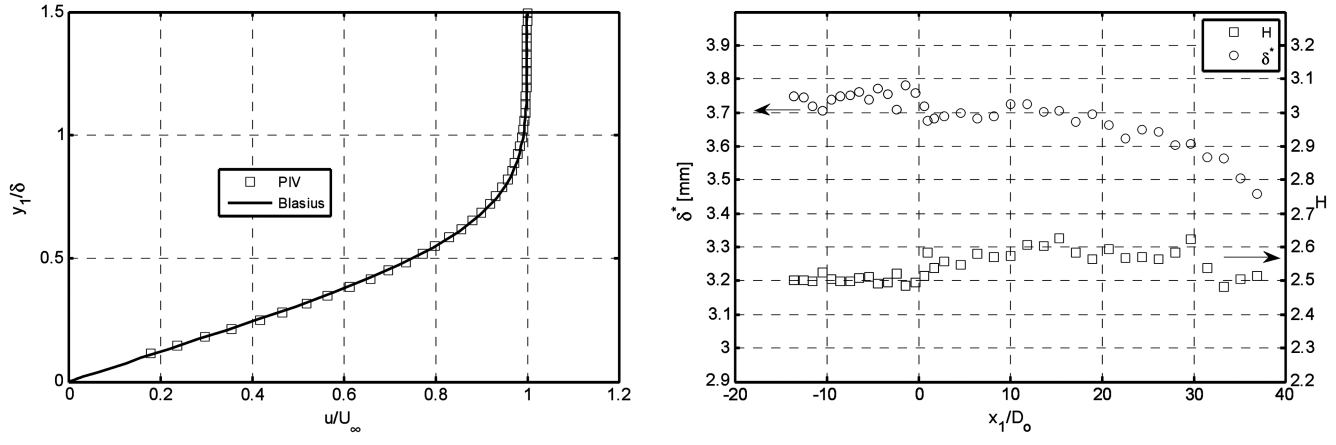

a) **b)**

Fig. 7 Shown are the following: a) boundary layer velocity profile at the location of the synthetic jet array, and b) distributions of displacement thickness and shape factor in the streamwise direction.

velocity field obtained by averaging 500 consecutive frames of PIV images taken at 5 Hz and with a 0.36×0.36 mm^2 interrogation area. The local boundary-layer thickness is about 10 mm. The velocity profile of the boundary layer at a distance of 10 mm upstream of the synthetic jet orifices is shown in Fig. 7a. The profile is close to the Blasius profile, confirming that the boundary layer is a zero-pressure-gradient laminar boundary layer. The streamwise distribution of boundary-layer displacement thickness indicates that the boundary layer becomes thinner as it approaches the inclined plate (Fig. 7b). However, the shape factor stays relatively constant, because the boundary layer does not separate for another $20D_o$ further along the inclined plate.

B. Dimensionless Parameters of Synthetic Jets Issued into a Boundary Layer

In the present experiment, both the spacing between adjacent orifices of the synthetic jet array and the distance between the array and the start of the inclined plate are fixed. Based on dimensional analysis, the behavior of synthetic jets issued into a given boundary layer is determined by the dimensionless stroke length L, the Reynolds number defined based on the stroke length Re_L, the jet-to-freestream velocity ratio (VR), and the Strouhal number Str.

The dimensionless stroke length is defined as

$$L = \frac{L_o}{D_o} = \frac{\bar{U}_o T}{D_o} \tag{1}$$

where L_o is the stroke length, which, according to the slug model [15], represents the length of the fluid column expelled during the blowing stroke; $\bar{U}_o$ is the time-averaged blowing velocity over the entire actuation cycle. It is also reported that, when L is greater than 4, the excessive vorticity produced in the blowing cycle, which can not be contained the primary vortex ring, will be shed, forming the secondary vortex ring trailing behind the primary ring [15,16].

The Reynolds number based on the stroke length is defined as

$$Re_L = \frac{\bar{U}_o L_o}{\nu} \tag{2}$$

Re_L is proportional to the vortex circulation in the vortex ring and hence quantifies the strength of a synthetic jet. It is therefore an important parameter for flow separation control applications in which fluid entrainment and mixing in the near-wall region via the generation of coherent vorticity is ultimately required.

The jet-to-freestream velocity ratio is defined as

$$\mathrm{VR} = \frac{\bar{U}_o}{U_\infty} \tag{3}$$

where U_∞ is the freestream velocity. VR indicates the relative strength between the jet and freestream velocity and affects the trajectory of the vortical structures as they propagate through the boundary layer [12,14]. In the current study, because the geometry of the synthetic jet actuator is fixed and the freestream velocity is constant, VR depends only on the displacement and oscillation frequency of diaphragm.

The Strouhal number defined based on the freestream velocity and the thickness of the undisturbed boundary layer at the orifices

$$Str = \frac{f\delta}{U_\infty} \tag{4}$$

is a useful dimensionless frequency for synthetic jets issued into a boundary layer. Assuming that the structures travel at the freestream

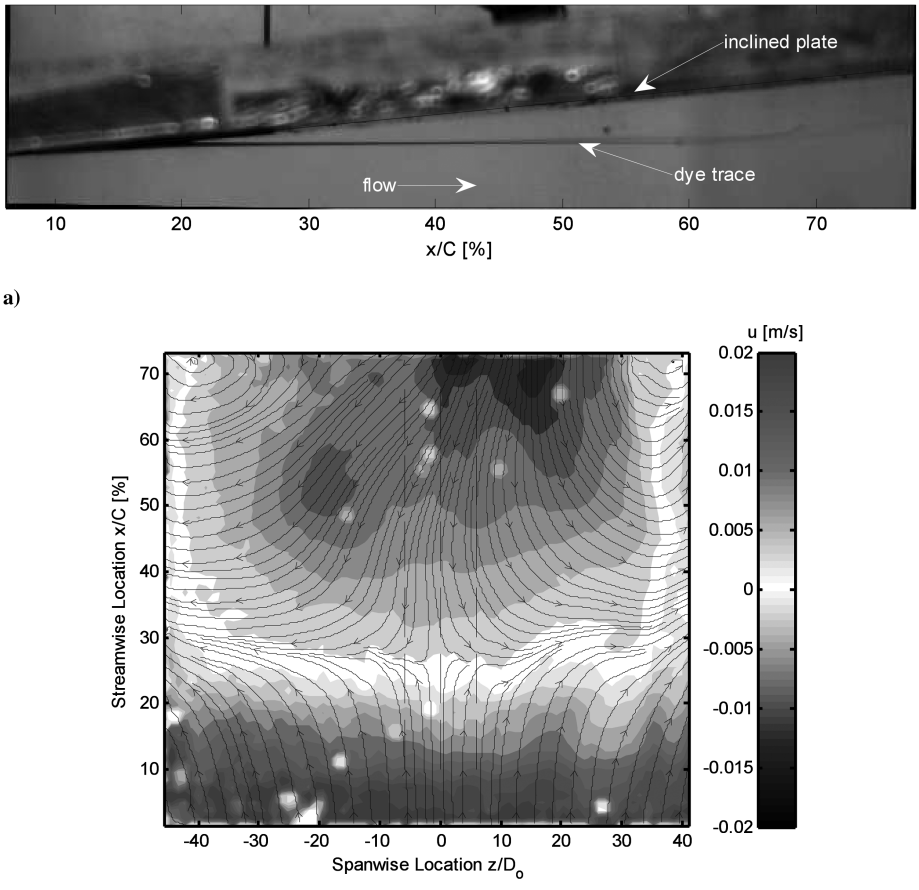

Fig. 8 Shown are the following: a) dye visualization of the flow separation over the inclined plate without active control, and b) time-averaged streamwise velocity contour and streamlines on a plane parallel to the inclined plate for the baseline case without the actuation of synthetic jets (flow is from bottom to top).

velocity, Str^{-1} is a measure of the distance between the consecutive structures produced by the synthetic jets as a fraction of the local boundary-layer thickness. As the convection velocity of the vortical structures is found to vary greatly between $0.5U_\infty$ and $0.96U_\infty$ for different synthetic jet operating conditions in the present experiment, U_∞ is used to define the Strouhal number for consistency.

C. Operational Conditions of Synthetic Jets

In the present experiment, the flow in the actuator can be adequately assumed to be incompressible. It can be proven that by flow continuity the mean time-averaged blowing velocity during the entire cycle across the orifice exit for the actuator studied in this paper is given by

$$\bar{U}_o = \frac{1}{3} f \Delta \left(\frac{D_c}{D_o} \right)^2 \tag{5}$$

where f is the oscillating frequency and Δ is the peal-to-peak displacement of the diaphragm. Equation (5) indicates that for the present actuator $\bar{U}_o$ is proportional to the diaphragm oscillation frequency and displacement. In addition, substituting Eq. (5) into Eq. (1), one can show that the dimensionless stroke length is independent of the diaphragm frequency; hence, it is proportional to the diaphragm displacement only. In this paper, the dimensionless parameters are calculated using the predicted $\bar{U}_o$ given in Eq. (5). In some published papers, the peak exit velocity is used to define VR. For the actuator used in the present study, the peak exit velocity is π times $\bar{U}_o$.

To investigate the flow control effectiveness of the synthetic jets in a range of actuator operating conditions, the diaphragm oscillating frequency is set at 1 Hz and then from 2 to 16 Hz with an increment of 2 Hz. At each frequency, the displacement is varied to yield a range of dimensionless stroke length from 1 to 16 with an increment of 1. These settings result in a velocity ratio ranging from 0.04 to 5.12 and

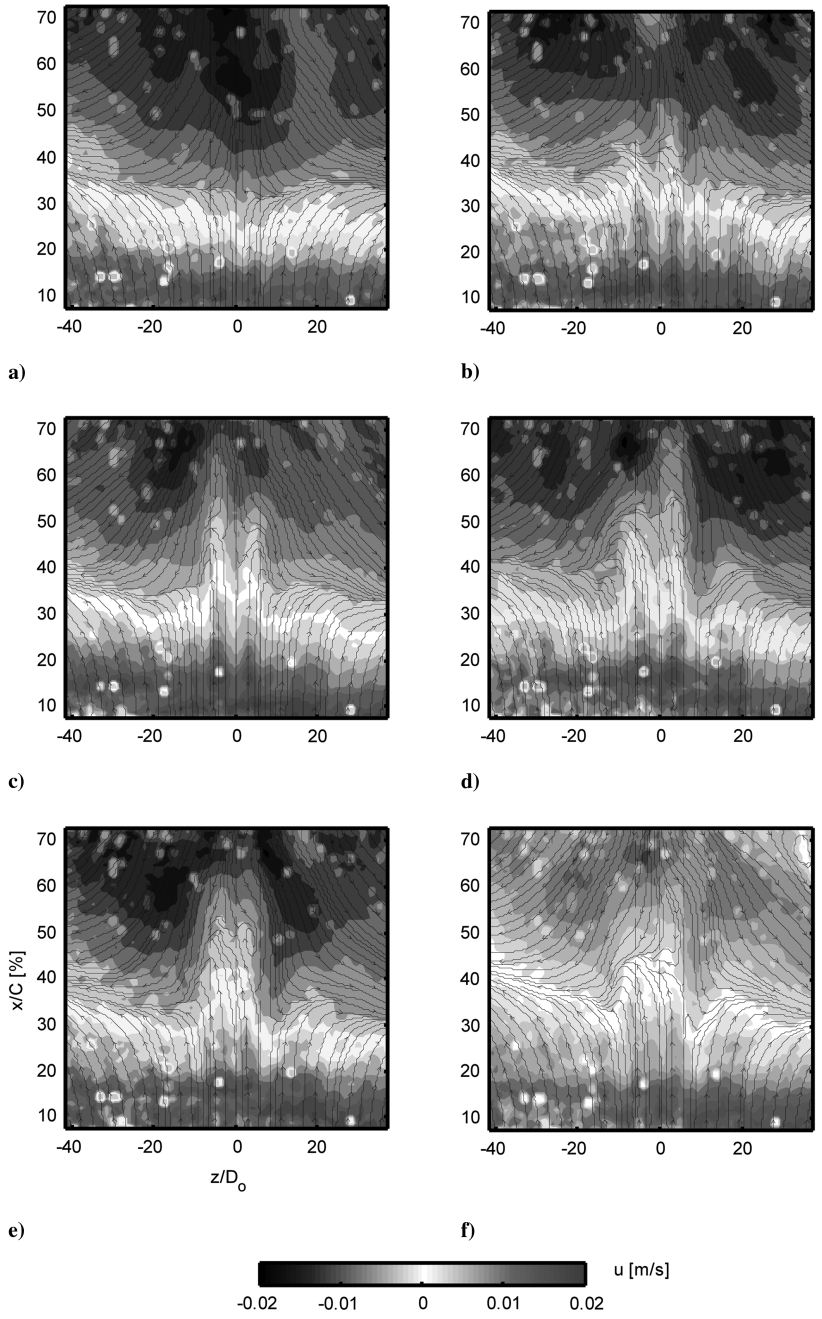

Fig. 9 Contours and streamlines of averaged velocity on a plane parallel to the inclined plate showing the footprint induced by synthetic jet actuators operated at $f = 2$ Hz ($Str = 0.2$): a) $L = 3$, VR = 0.12; b) $L = 6$, VR = 0.24; c) $L = 8$, VR = 0.32; d) $L = 12$, VR = 0.48; e) $L = 14$, VR = 0.56; and f) $L = 16$, VR = 0.64 (dashed lines mark the central lines of three synthetic jets; flow is from bottom to top).

a Reynolds number ranging from 4 to 16,384. As the actuation frequency increases from 1 to 16 Hz, Str increases from 0.1 to 1.6.

In the present setup, the highest frequency of Tollmien–Schlichting wave is estimated to be around 0.67 Hz. Because the minimum actuator operating frequency is 1 Hz, the synthetic jet is not expected to trigger the boundary-layer instability unless the strength of the jets becomes very strong. From a hot-film measurement, the shear-layer frequency in the separated flow is found to be around 0.4 Hz. Hence, the coupling between the actuation frequency and the shear-layer frequency will not occur.

IV. Results and Discussions

A. Baseline Flow

In the present setup, a thin rubber sheet is used to provide a smooth transition from the horizontal plane to the 5 deg inclined plate. Hence, the flow does not separate at the curved joint between the two plates; instead, it separates at some distances further downstream. Dye was injected from a 1-mm-diam port located at a short distance upstream of the separation point on the central plane of the inclined plate to reveal the location of separation in the baseline case without the actuation of the synthetic jets. From the dye visualization image shown in Fig. 8a, it can be seen that the dye becomes detached from the test surface at about 20% of the chord length of the inclined plate, C, from the start of the inclined plate.

The contour of time-averaged streamwise velocity together with the streamlines on the PIV measurement plane parallel to the inclined plate for the baseline case is shown in Fig. 8b. The location of separation line can be identified as the region where the streamlines coming from upstream begin to divert sideways. It can be seen that the separation line is located at about 27%C downstream of the start of the inclined plate, which is slightly further downstream than that indicated by the dye in Fig. 8a. This discrepancy is believed to be caused by the laser sheet being located 1.5 mm away from the inclined plate where the velocity is slightly higher. Nevertheless, for the purpose of evaluating the effectiveness of synthetic jets operated

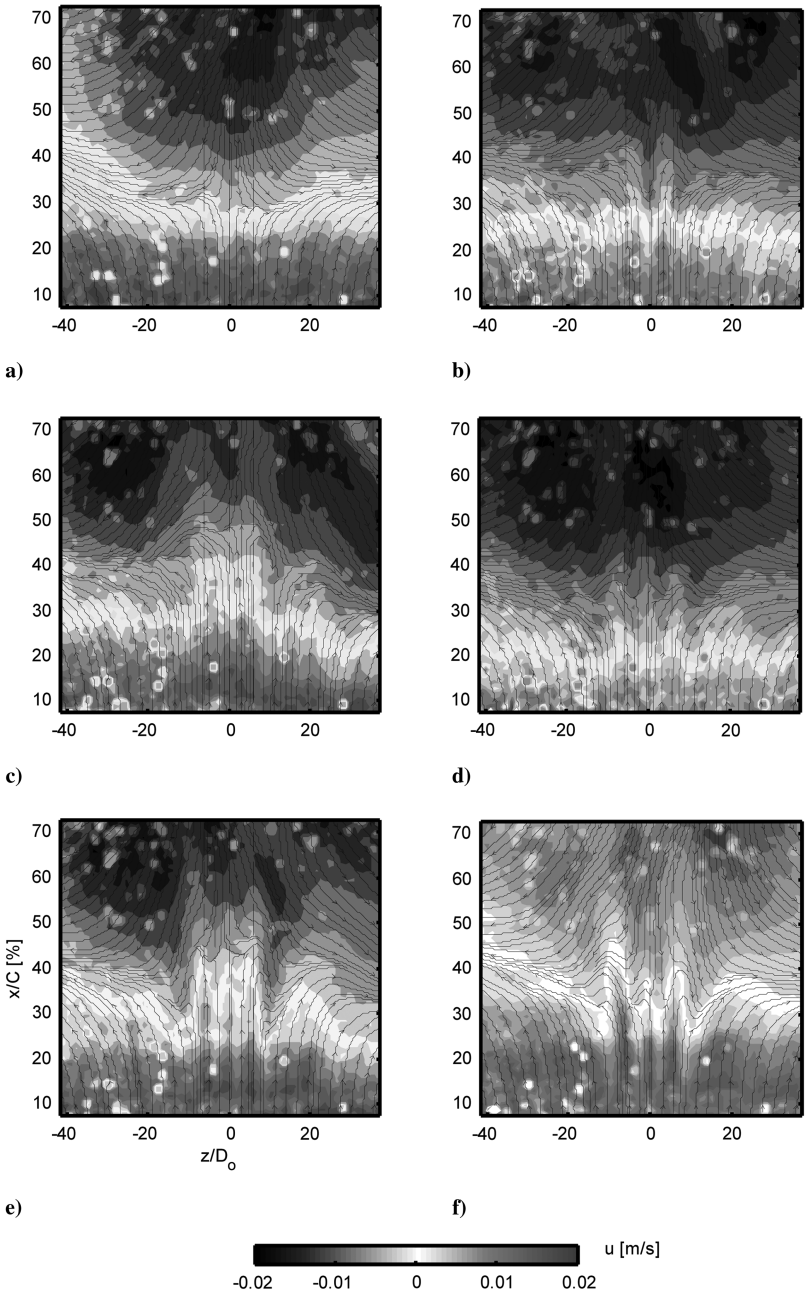

Fig. 10 Contours and streamlines of averaged velocity on a plane parallel to the inclined plate showing the footprint induced by synthetic jet actuators operated at $f = 4$ Hz ($Str = 0.8$): a) $L = 2$, VR $= 0.16$; b) $L = 3$, VR $= 0.24$; c) $L = 6$, VR $= 0.48$; d) $L = 8$, VR $= 0.64$; e) $L = 11$, VR $= 0.88$; and f) $L = 15$, VR $= 1.2$ (dashed lines mark the central lines of three synthetic jets; flow is from bottom to top).

at different conditions in delaying separation, this is not an issue because the PIV results obtained at the same measurement plane will be compared.

B. Footprints of Synthetic Jets in the Separated Flow

To assess the flow control effect of synthetic jets operated at different conditions, the contours of time-averaged streamwise velocity superimposed with the streamlines on the PIV measurement plane parallel to the inclined plate are examined. Because of the limited space in this paper, only the results at $f = 2, 4$, and 12 Hz are shown in detail. At each frequency, the dimensionless stroke length is increased from 1 to 16 as the result of an increasing diaphragm displacement.

At $f = 2$ Hz, there is no visible separation delay at $L = 3$ and VR $= 0.12$ (see Fig. 9a). As L increases to 6 and VR to 0.24, a separation delay near the central region can be observed (see Fig. 9b). It becomes more obvious at $L = 8$ and VR $= 0.32$ where the delayed separation is associated with the appearance of two high-speed streaks, for which the spanwise locations are aligned with the middle points between adjacent synthetic jets (see Fig. 9c). A slightly further delay in separation is seen at $L = 12$ (VR $= 0.48$) and 14 (VR $= 0.56$) (see Figs. 9d and 9e). The effect of separation delay appears to be slightly worsened at $L = 16$ and VR $= 0.64$ (see Fig. 9f). In all the cases at $f = 2$ Hz, the delay of separation is associated with the appearance of two high-speed streaks that originate upstream.

At $f = 4$ Hz, although a visible separation delay is not seen at $L = 2$ and VR $= 0.16$ (see Fig. 10a), it appears at $L = 3$ and VR $= 0.24$ along with the appearance of two high-speed streaks (see Fig. 10b). The separation is delayed further as L increases to 6 and VR to 0.48 (see Fig. 10c). Interestingly, the level of separation delay reduces at $L = 8$ and VR $= 0.64$ with the emergence of a three-streak pattern (see Fig. 10d). The three streaks appear to be aligned

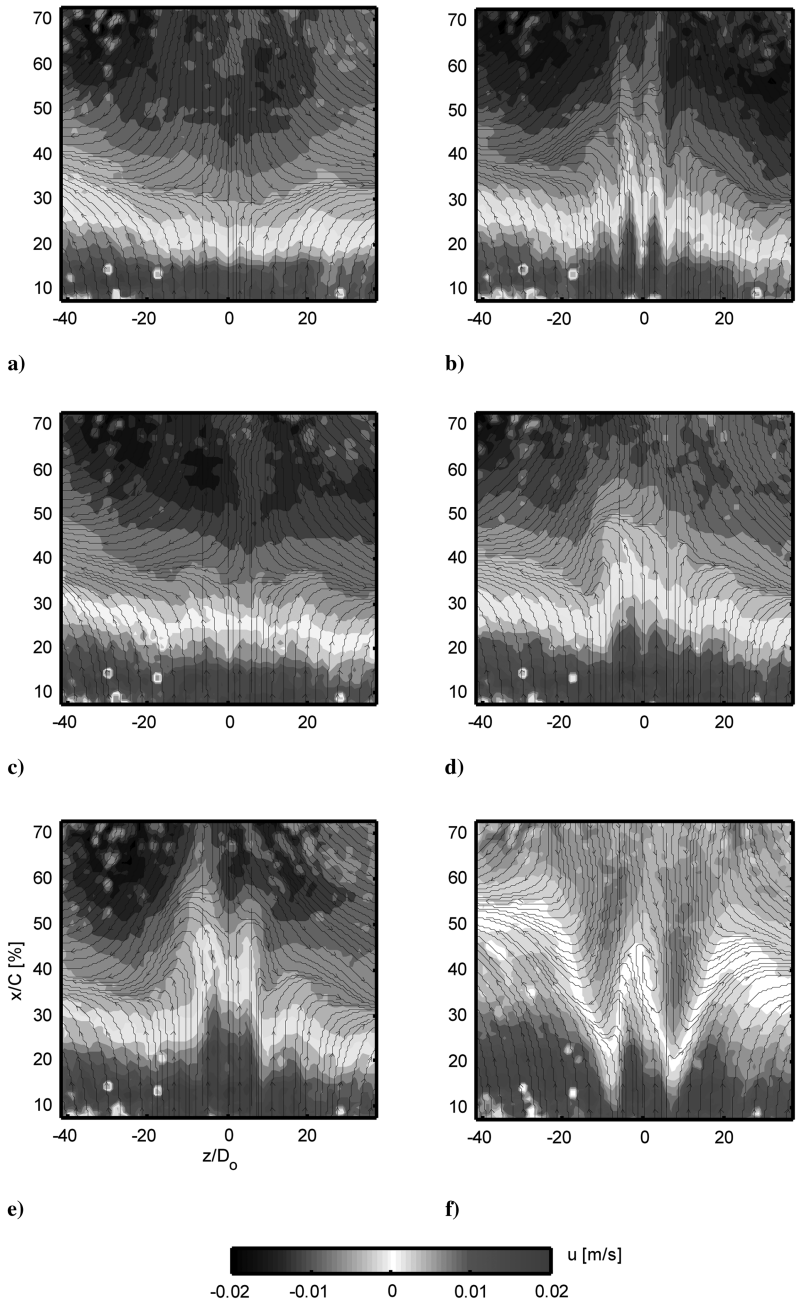

Fig. 11 Contours and streamlines of averaged velocity on a plane parallel to the inclined plate showing the footprint induced by synthetic jet actuators operated at $f = 12$ Hz ($Str = 1.2$): a) $L = 1$, VR $= 0.24$; b) $L = 2$, VR $= 0.48$; c) $L = 3$, VR $= 0.72$; d) $L = 5$, VR $= 1.2$; e) $L = 6$, VR $= 1.44$; and f) $L = 8$, VR $= 1.92$ (dashed lines mark the central lines of three synthetic jets; flow is from bottom to top).

with the centers of the three synthetic jets. The level of separation delay peaks up again at $L = 11$ and VR $= 0.88$ (see Fig. 10e). It then drops slightly as L and VR increase further to $L = 15$ and VR $= 1.2$ (see Fig. 10f).

At $f = 12$ Hz, no visible separation delay is observed at $L = 1$ and VR $= 0.24$ (see Fig. 11a). A pronounced separation delay is then seen at $L = 2$ and VR $= 0.48$ along with the two-streak pattern (see Fig. 11b). The separation delay disappears at $L = 3$ (VR $= 0.72$) and $L = 4$ (VR $= 0.96$), but it reappears with a two-streak pattern as L increases to 5 (VR $= 1.2$) (see Figs. 11c–11e). As L increases further, the two streaks merge to a single streak. The synthetic jets become so strong that they begin to affect the entire separated flow by causing a strong reverse flow in the region immediately outside the jet array and a significant separation delay in the flow further outboard (see Fig. 11f). According to Crook [17], the synthetic jets become turbulent when the ratio of the jet peak velocity to the freestream velocity exceeds 4 (equivalent to VR $= 1.27$). Hence, the global alternation of the separated flow observed at high VR in the present experiment is likely to be associated with the breakdown of the laminar boundary layer into turbulent caused by the strong turbulent synthetic jets.

Figure 12 shows the mapping of the flow patterns observed in the separated flow for all operating conditions. Different flow patterns are indicated using different symbols and four constant VR lines are added to assist the interpretation of results. It is seen that, at a velocity ratio of less than about 0.3, the control effect is not appreciable. A VR between 0.3 and 0.5 results in a separation delay associated with the presence of a two-streak flow pattern. A velocity ratio greater than 1.5 appears to provoke a global alternation of the separated flow. Between VRs of about 0.5 and 1.5, the observed flow patterns appear to vary with the actuation frequency. At $f \leq 2$ Hz, the two-streak flow pattern seems to persist up to $L = 16$, whereas at 4 Hz $\leq f \leq$ 8 Hz the three-streak pattern is prevalent. At $f \geq 10$ Hz, the separation delay effect disappears between $0.5 <$ VR < 1 and it reappears with a two-streak pattern at VR > 1. The two-streak pattern at VR > 1 may not necessarily be produced by the same type of vortical structures that produce the two-streak pattern at $0.3 <$ VR < 0.5. The vortical structures at high VRs and frequencies are expected to be complex due to the presence of secondary/tertiary structures and the interaction between consecutive structures in the streamwise direction.

C. Vortical Structures Produced by Synthetic Jets Responsible for Delaying Separation

To achieve a better understanding of the vortical structures that are responsible for the production of the typical streak patterns that delay separation, LIF images were obtained on the central streamwise plane across the middle synthetic jet in the boundary layer upstream of the inclined plate. Because the dye diffused rapidly at large dimensionless stroke lengths, the results are limited to L of less than 5. As the LIF images are only available at the central plane of the middle orifice, they cannot capture the structures that are located off the center. However, because the interaction between the adjacent synthetic jets at the spacing tested in the present experiment is weak, the LIF images can be interpreted in light of the well-established findings from the dye visualization and numerical simulations of single jets obtained in previously published works [12–14].

Figures 13–15 show the LIF images taken on the central streamwise plane across the middle synthetic jet for a few selected cases. At $f = 4$ Hz and $L = 3$ (see Fig. 13a), the vortical structures appear as highly stretched hairpin vortices propagating within the undisturbed boundary layer similar to those observed by Jabbal and Zhong [12]. However, because the strength of the synthetic jets is relatively weak in this case due to their low Reynolds number ($Re_L = 144$), they do not produce a noticeable separation delay. At $f = 4$ Hz and $L = 4$, the structure first appears as a stretched vortex ring with a pair of trailing legs (see Fig. 13b). Its upstream branch is weakened as the structure propagates downstream and it eventually

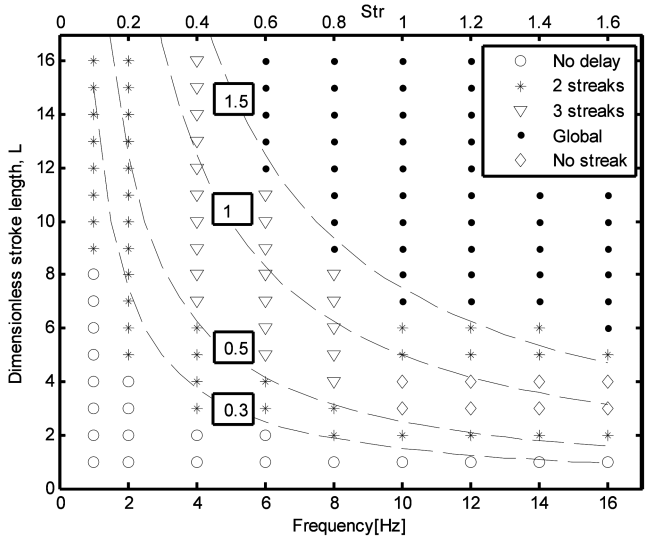

Fig. 12 Parameter space of different types of footprints produced by synthetic jets on the inclined plate (dashed lines: VR = constant).

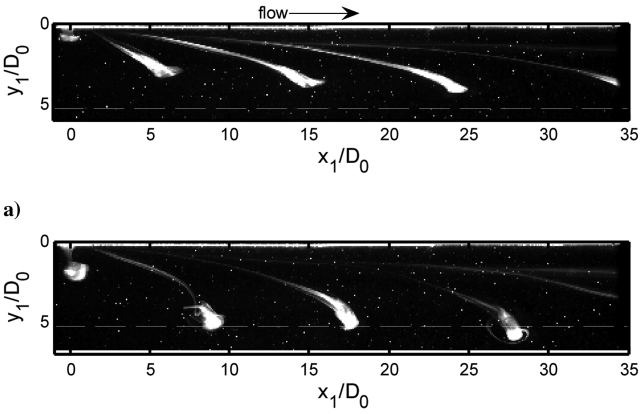

Fig. 13 LIF visualization on the central plane of the middle synthetic jet operated at $f = 4$ Hz ($Str = 0.4$): a) $L = 3$, VR $= 0.24$; and b) $L = 4$, VR $= 0.32$ (dashed line: edge of undisturbed boundary layer).

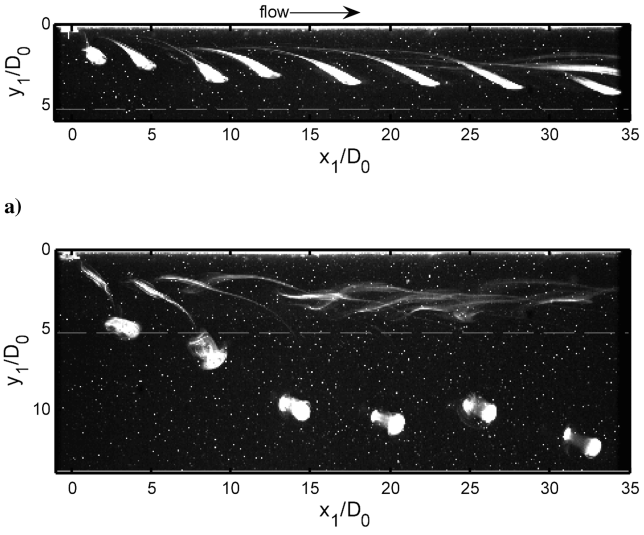

Fig. 14 LIF visualization on the central plane of the middle synthetic jet operated at $f = 8$ Hz ($Str = 0.8$): a) $L = 2$, VR $= 0.32$; and b) $L = 4$, VR $= 0.64$ (dashed line: edge of undisturbed boundary layer).

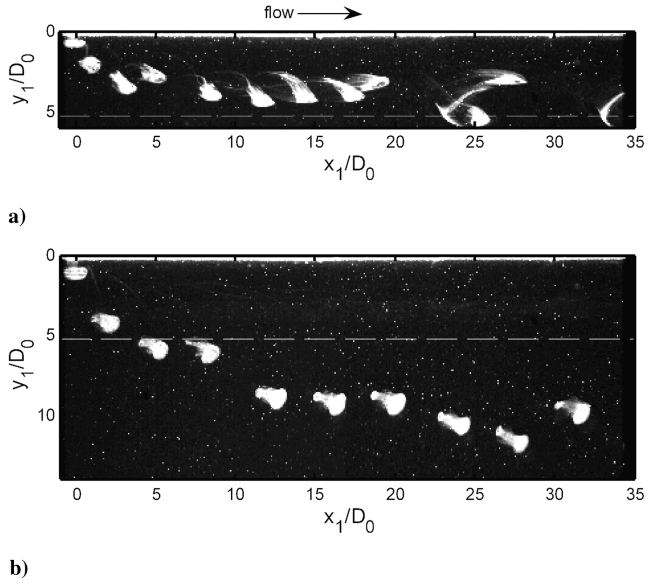

Fig. 15 LIF visualization on the central plane of the middle synthetic jet operated at $f = 12$ Hz ($Str = 1.2$): a) $L = 2$, VR = 0.48; b) $L = 3$, VR = 0.72 (dashed line: edge of undisturbed boundary layer).

turns into a hairpinlike structure. In general, the resultant hairpin structures are similar to those observed at $L = 3$ but they are stronger due to a higher Re_L ($Re_L = 400$). Hence, their impact on the separated flow is more pronounced.

At $f = 8$ Hz and $L = 2$ (Fig. 14a), the vortical structures appear to be similar to the hairpin vortex structures seen at $f = 4$ Hz and $L = 2$ (Fig. 13b), which are responsible for the two-streak pattern observed in the separated flow region. Although each hairpinlike structure is expected to produce a pair of high-velocity streaks based on the results from a single synthetic jet, in this case only two high-velocity streaks are clearly observed in the separated flow with one on each side of the middle jet in the three-jet array. To help in understanding the formation of this pattern, the contours of surface shear stress upstream of the start of the inclined plate and the surface friction lines over the inclined plate for the case of $f = 8$ Hz and $L = 2$ from the CFD simulations by Zhou and Zhong [18] are shown in Fig. 16a. It is seen that the regions of high surface shear stress produced by the adjacent jets, which are equivalent to regions of high velocity, merge with each other at some distances downstream of the orifices, resulting in a strong single high-speed region midway between two adjacent jets. In contrast, the high-speed region outboard of each of the two side orifices is considerably weaker, producing a much weaker delay of flow separation. Hence, the array of three jets produces the two-streak flow pattern that is observed in the experiment as illustrated in Fig. 17. The difference in the pattern of high-speed streaks observed at the inboard and outboard of each side jet can also be taken as evidence showing the different effect produced by a single jet and a jet in an array with moderate jet spacing. Here the near-wall impact of a jet in an array is much stronger due to the merger of vortical structures from the neighboring jets.

At $f = 8$ Hz and $L = 4$, where a weak three-streak pattern is observed, the vortical structures appear as typical tilted vortex ring type structures (see Fig. 14b) previously identified by Jabbal and Zhong [12] and Zhou and Zhong [13]. As shown by the simulation results of Zhou and Zhong [18] (see Fig. 16b), each tilted vortex ring type structure produces a high-speed streak on the central plane downstream of each orifice. In addition, the merger of high-speed streaks from adjacent orifices is only moderate such that each individual high-speed streak remains distinct and their strength appears similar. Hence, the array of three jets will produce the three-streak flow pattern that delays separation as shown in Fig. 18.

At $f = 12$ Hz and $L = 2$ (Fig. 15a), although much more closely spaced, the stretched vortex ring type vortical structures appear similar to those seen at $f = 4$ Hz and $L = 4$ (Fig. 13b). Hence, it is not surprising that the two-streak pattern is also observed in the separated flow region. At $f = 12$ Hz and $L = 3$, where limited separation delay and no appreciable flow pattern is observed, the vortical structures appear as typical tilted vortex ring type structures (Fig. 15b).

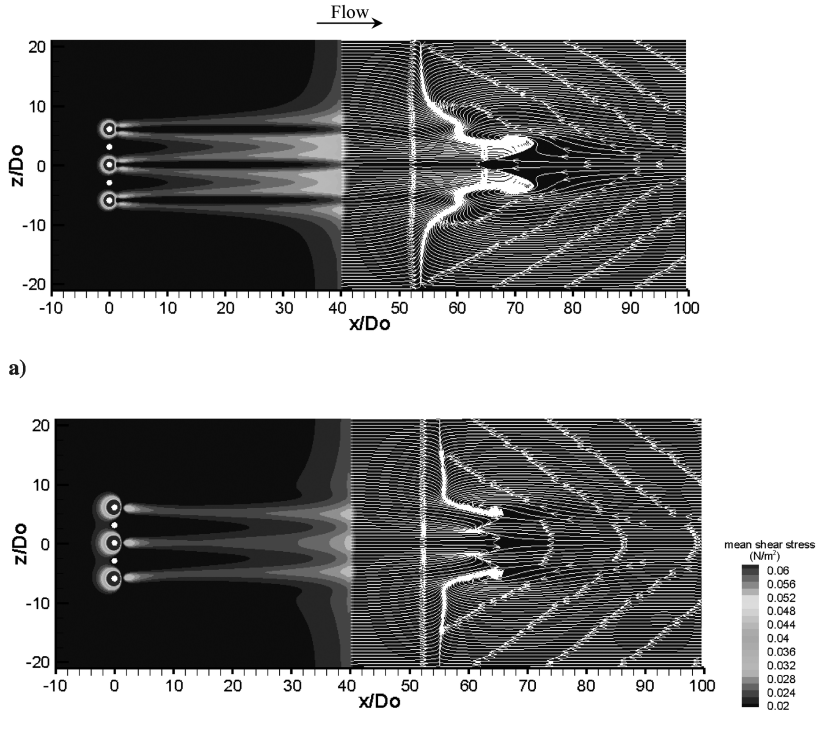

Fig. 16 Contours of surface shear stress upstream of the start of the inclined plate located at $x/D_o = 40$ and the surface friction lines over the inclined plate obtained from CFD simulations at $f = 8$ Hz ($Str = 0.8$): a) $L = 2$, VR = 0.32; and b) $L = 4$, VR = 0.64.

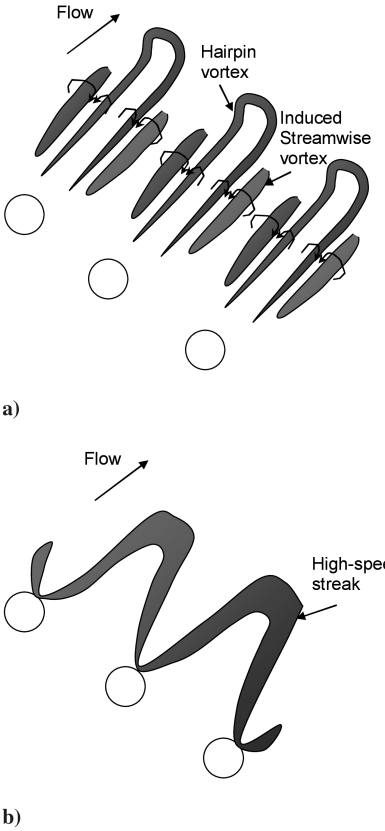

Fig. 17 Schematic drawings: a) hairpin vortices and their induced vortices produced by the synthetic jet array, and b) two high-speed streaks produced by the array.

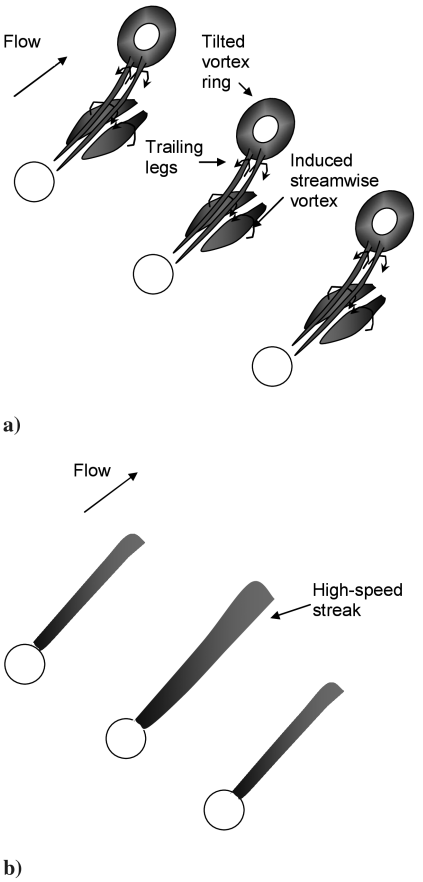

Fig. 18 Schematic drawings: a) tilted vortex rings and their induced vortices produced by the synthetic jet array, and b) three high-speed streaks produced by the array.

D. Evaluation of Flow Control Effectiveness

To evaluate the flow control effectiveness of synthetic jet array quantitatively, the streamwise location of the space-averaged separation line along a spanwise width of $6D_o$ across the middle jet centrally is calculated and then normalized by the length of the inclined plate. Because the spanwise spacing between adjacent orifices is $6D_o$, the aforementioned choice of spanwise width essentially allows the flow control effectiveness of the middle jet in the array to be examined. The flow control effectiveness is presented as a contour in the space of dimensionless stroke length and diaphragm frequency in Fig. 19. The flow patterns observed in the separated flow are also added to assist the interpretation of the results.

According to the flow patterns observed in the separated flow, the map of flow control effectiveness of the synthetic jet array can be roughly divided into four zones based on the value of VR. At VR less than 0.3, the flow control effectiveness is not appreciable. Within the zone of $0.3 < \mathrm{VR} < 0.5$, a good flow control effect is achieved at all frequencies at which a two-streak flow pattern is observed. The strong effect of separation delay obtained at $\mathrm{VR} > 1.5$ is not of interest in the present study because it is believed to be caused by the breakdown of the laminar flow into turbulent flow. For $0.5 < \mathrm{VR} < 1.5$, the flow control effect is largely associated with the presence of tilted vortex ring type structures and the level of flow control effectiveness appears to experience two peaks located at different values of L as the frequency increases. The first peak at $10 < L < 12$ observed at $f = 4$ Hz is caused by the gradual strengthening of the tilted vortex ring type structures and the subsequent weakening of their near-wall effect when they are located further away from the wall as L increases (seen earlier in Fig. 10). On the other hand, because as the frequency increases the dimensionless stroke length for achieving the same range of VRs decreases, the variation in the flow control effectiveness observed is likely to be caused by the combined effect of the strength of the tilted vortex ring type structures and their relative position to the wall as L changes. As such, a second peak occurs at $5 < L < 6$ and $4\ \mathrm{Hz} < f < 12\ \mathrm{Hz}$ due to a favorable combination of the strength of the tilted vortex ring type structures and their relative position to the wall at this particular L. The disappearance of flow control effect at $3 < L < 4$ could be due to the weakening of the vortical structures as L increases further. The almost invisible secondary and tertiary structures from the LIF images shown in Fig. 15b may lend some support to this hypothesis. In general, the tilted vortex ring type structures at large VRs are usually quite complex due to the distortion of vortical structures. CFD simulation results of some of these cases are being examined to obtain a better understanding of the hierarchy of vortices and their flow control effect.

It is also observed that, as the frequency increases from 1 to 16 Hz, a stronger flow separation delay appears to be associated first with the two-streak pattern, then with the three-streak pattern, and finally with the two-streak pattern again. Such a switching between the hairpins and the tilted vortex rings in producing a stronger control effect as the frequency increases is believed to be caused by the changes in the strength of hairpin vortices. At low frequencies ($f \leq 6$ Hz), a dimensionless stroke length greater than 4 is required to produce $\mathrm{VR} = 0.3 \sim 0.5$, resulting in the formation of strong stretched vortex ring type structures with secondary trailing vortices. As the frequency increases, the value of L required for producing $\mathrm{VR} = 0.3 \sim 0.5$ reduces to less than 4 and the strength of the stretched vortex rings weakens such that in comparison the tilted vortex rings formed at higher L become more effective. As the frequency increases further, the consecutive stretched vortex rings are closely packed together, resulting in a stronger effect in the near-wall region although they are relatively weak individually.

Overall, the vortical structures that produce the two-streak patterns offer a stronger effect of separation delay than those that produce the three-streak pattern in most cases. This is likely because that the hairpin type structures are more effective than the tilted vortex ring type structures due to their proximity to the wall. The authors believe that a key mechanism of separation delay is to increase mixing by

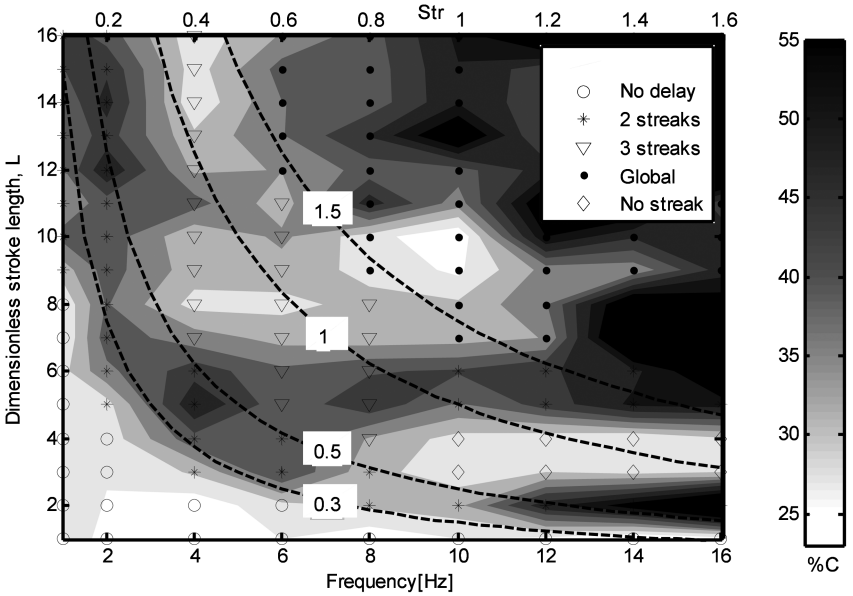

Fig. 19 Contours of separation control effect at various frequencies and stroke lengths (dashed lines: VR = constant).

introducing coherent structures into the boundary layer that subsequently entrain high-speed fluid from the outer part of the boundary layer to the near-wall region. A high VR results in vortical structures which penetrate the boundary layer within a short distance downstream, producing a limited impact in the near-wall region in the far-field at the expense of higher power consumption. Whereas at a relatively low VRs, the structures remain within the boundary layer and persist further downstream; hence, they are likely to be more effective in enhancing mixing, provided that they have sufficient vorticity strength. Zhou and Zhou [18] compared the flow control effectiveness of synthetic jets operated at different conditions and examined the variations of wall shear stress upstream of the separated flow using their CFD simulation results and confirmed the validity of this hypothesis.

Based on the results from the present study, it is seen that a flow control effect can be achieved with $0.3 \leq \mathrm{VR} < 1.5$, although the level of flow control effectiveness varies. This, in some way, explains why a wide range of VRs has been reported as being effective in the literature. However, the chosen setting in each individual experiment may not be optimized. An optimal actuator operating condition should be the one that delivers the maximum level of separation delay with the minimum energy expenditure.

The time-averaged total power consumption of the synthetic jet actuator was obtained by measuring the temporal variations of current and voltage supplied to the shaker. It includes the power required to overcome the pressure difference across the oscillating diaphragm, to drive the mass of the diaphragm assembly to undergo a sinusoidal motion at a given frequency and displacement, to work against the deformation of the rubber diaphragm, and to overcome the mechanical and electrical losses in the shaker. As it is shown in Fig. 20, over the experimental range the power consumption increases more sharply with an increasing diaphragm displacement than with an increasing frequency such that at the same VR the power consumption is lower when the actuator is operated at a higher frequency. For the present actuator, the diaphragm resonant frequency and Helmholtz resonant frequency are found to be around 300 and 1400 Hz, respectively, which are well above the diaphragm oscillating frequencies tested in this experiment. Hence, the reduced power consumption at the higher frequency range is not caused by the actuator being operated near these resonant frequencies.

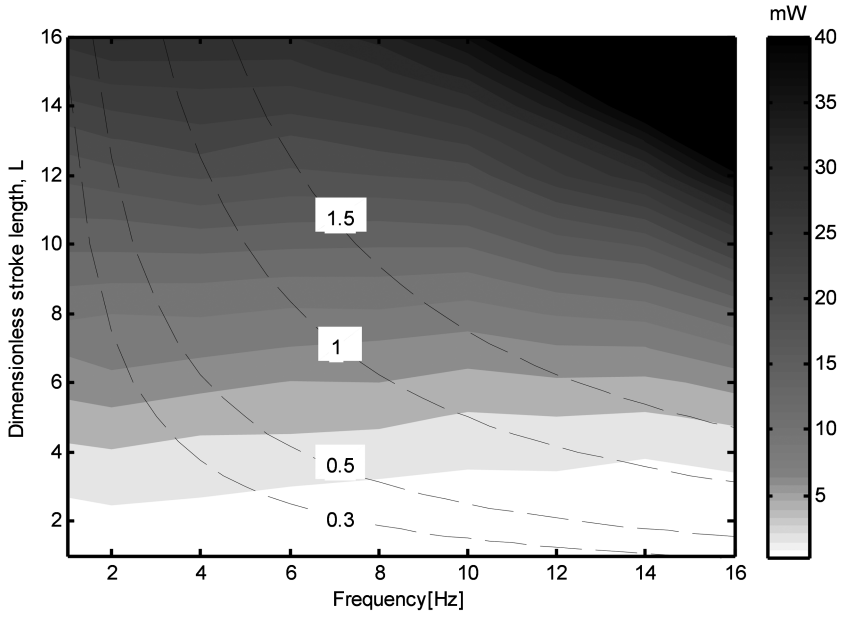

Fig. 20 Contour of power consumption of the synthetic jet actuator operated at different conditions (dashed lines: VR = constant).

In the present study, the best flow separation effect is obtained at the highest frequency ($f = 16$ Hz) and $L = 2$ (VR $= 0.5$ and $Str = 1.6$) at which the separation line is pushed downstream significantly. At this condition, the power consumption is maintained at a very low level. Therefore, among the actuator operating conditions tested in this study, the optimal condition is identified as $L = 2$, VR $= 0.5$, and $Str = 1.6$. When taking into account of the actual convection velocity of the vortical structures produced by the synthetic jets of $0.7U_\infty$, deduced from the LIF images, the spacing between the consecutive hairpinlike structures is found to be about 44% of the local boundary-layer thickness at the orifices of the synthetic jets. Nevertheless, as the level of interaction between neighboring synthetic jets and their flow control effectiveness are expected to alter upon changes in the jet spacing and the distance between the orifices and the baseline separation line, the generality of this finding remains to be established in future work.

V. Conclusions

An experimental study of flow control using an array of three synthetic jets ($D_o = 2$ mm) has been undertaken in a separated laminar flow over an inclined flat plate in a water channel. In this experiment, the spacing between the jets was fixed at $12D_o$ and the jet array was located at about $60D_o$ upstream of the baseline separation line. PIV was employed to obtain the information about the extent of flow separation delay over the inclined plate at different synthetic jet operating conditions. The laser-induced florescence flow visualization technique was also used to reveal the characteristics of the vortical structures produced by the synthetic jets upstream of the inclined plate, which result in a delay of separation.

It was observed that the flow separation delay is typically associated with the presence of two streaks or three streaks of high streamwise velocity in the separated flow. Based on the results from the present experiment, a parameter map indicating the flow pattern observed at different actuator operating conditions is produced. In addition, a contour map showing the separation control effectiveness at the corresponding conditions is also obtained. It was found that the two-streak flow pattern is produced at a VR between 0.3 and 0.5, whereas the three-streak pattern occurs at $0.5 < \text{VR} < 1.5$. The LIF images confirm that the two-streak flow pattern is caused by the hairpin type vortical structures produced by synthetic jets, whereas the three-streak pattern is caused by the tilted vortex ring type structures. For the range of actuator operating conditions tested in this study, operating the synthetic jets at L of around 2, a VR of around 0.5, and a Strouhal number of around 1.6, would deliver the best flow control effect with the least energy consumption. Under these conditions, hairpinlike vortical structures are observed with a streamwise spacing of 44% of the local boundary layer thickness at the location of the synthetic jets. Nevertheless, as the level of interaction between neighboring synthetic jets and their flow control effectiveness are expected to alter upon changes in the jet spacing and the distance between the orifices and the baseline separation line, the generality of this finding remains to be established in future work.

Acknowledgments

The authors would like to acknowledge the financial support from the Engineering and Physical Sciences Research Council in the United Kingdom of the work reported in this paper. They would also like to thank Fushui Guo for designing the test plate and the synthetic jet actuator used in this experiment and Jue Zhou for providing her CFD simulation results for comparison.

References

[1] Glezer, A., and Amitay, M., "Synthetic Jets," *Annual Review of Fluid Mechanics*, Vol. 34, 2002, pp. 503–529. doi:10.1146/annurev.fluid.34.090501.094913

[2] Zhong, S., Jabbal, M., Tang, H., Garcillan, L., Guo, F., Wood, N. J., and Warsop, C., "Towards the Design of Synthetic-Jet Actuators for Full-Scale Flight Conditions. Part 1: The Fluid Mechanics of Synthetic-Jet Actuators," *Flow, Turbulence and Combustion*, Vol. 78, No. 3, 2007, pp. 283-307. doi:10.1007/s10494-006-9064-0

[3] Tang, H., Zhong, S., Jabbal, M., Garcillan, L., Guo, F., Wood, N. J., and Warsop, C., "Towards the Design of Synthetic-Jet Actuators for Full-Scale Flight Conditions. Part 2: Low-Dimensional Actuator Prediction Models and Actuator Design Methods," *Flow, Turbulence and Combustion*, Vol. 78, No. 3, 2007, pp. 309–329. doi:10.1007/s10494-006-9061-3

[4] Ho, C.-M., and Tai, Y. C., "Review: MEMS and Its Applications for Flow Control," *Journal of Fluids Engineering*, Vol. 118, 1996, pp. 437–447. doi:10.1115/1.2817778

[5] Gad-el-Hak, M., "Modern Developments in Flow Control," *Applied Mechanics Reviews*, Vol. 49, No. 7, 1996, pp. 365–379. doi:10.1115/1.3101931

[6] McMichael, J. M., "Progress and Prospects for Active Flow Control Using Micro-Fabricated Electro-Mechanical Systems (MEMS)," AIAA Paper 96-0306, 1996.

[7] Crook, A., Sadri, A. M., and Wood, N. J., "The Development and Implementation of Synthetic Jets for the Control of Separated Flow," AIAA Paper 99-3176, 1999.

[8] Amitay, M., Smith, D. R., Kibens, V., Parekh, D. E., and Glezer, A., "Modification of the Aerodynamic Characteristics of an Unconventional Airfoil Using Synthetic Jet Actuators," *AIAA Journal*, Vol. 39, No. 3, 2001, pp. 361–370. doi:10.2514/2.1323

[9] McCormick, D. C., "Boundary Layer Separation Control with Directed Synthetic Jets," AIAA Paper 2000-0519, 2000.

[10] Dandois, U., Garnier, E., and Sagaut, P., "Numerical Simulation of Active Separation Control by a Synthetic Jet," *Journal of Fluid Mechanics*, Vol. 574, 2007, pp. 25–58. doi:10.1017/S0022112006003995

[11] Gilarranz, J. L., Traub, L. W., and Rediniotis, O. K., "A New Class of Synthetic Jet Actuators. Part II. Application to Flow Separation Control," *Journal of Fluids Engineering*, Vol. 127, 2005, p. 377. doi:10.1115/1.1882393

[12] Jabbal, M., and Zhong, S., "The Near-Wall Effect of Synthetic Jets in a Boundary Layer," *International Journal of Heat and Fluid Flow*, Vol. 29, No. 1, 2008, pp. 119–130. doi:10.1016/j.ijheatfluidflow.2007.07.011

[13] Zhou, J., and Zhong, S., "Numerical Simulations of the Interaction of Circular Synthetic Jets with A Boundary Layer," *Computers & Fluids*, Vol. 38, 2009, pp. 393–405. doi:10.1016/j.compfluid.2008.04.012

[14] Zhong, S., Millet, F., and Wood, N. J., "The Behaviour of Circular Synthetic Jets in a Laminar Boundary Layer," *The Aeronautical Journal*, Vol. 109, No. 1100, Oct. 2005, pp. 462–470.

[15] Smith, B. L., and Glezer, A., "The Formation and Evolution of Synthetic Jets," *Physics of Fluids*, Vol. 10, No. 9, 1998, pp. 2281–2297. doi:10.1063/1.869828

[16] Jabbal, M., Wu, J., and Zhong, S., "The Performance of Round Synthetic Jets in Quiescent Flow," *The Aeronautical Journal*, Vol. 110, No. 1108, 2006, pp. 385–393.

[17] Crook, A., "The Control of Turbulent Flows Using Synthetic Jets," Ph.D., Dissertation, School of Engineering, Univ. of Manchester, Manchester, England, U.K., 2002.

[18] Zhou, J., and Zhong, S., "Numerical Simulations of the Interaction of an Array of Synthetic Jets with a Separated Boundary Layer," *KATNet II Conference on Key Aerodynamic Technologies*, May, 2009.

A. Naguib
Associate Editor